Friday 27th April 2001 **9 – 12**

MODELLING OF MATERIALS (2) – possible Answers

SECTION A

1. (a) Expansion of the potential energy $U(r)$:

$$U(r) = \underbrace{\sum_i U_1(r_i)}_{\text{external field}} + \underbrace{\sum_i \sum_j U_2(r_i, r_j)}_{\text{pair term}} + \underbrace{\sum_i \sum_j \sum_k U_3(r_i, r_j, r_k)}_{\text{3–body term}} + \ldots$$

Axilrod–Teller potential improves the bonding in molecular solids – extends fluctuating dipoles between atom pairs to triplets. Limited, however, to weakly bonded covalent solids.

(b) Cooling curves, dilatometry, X–ray, metallography, electrical conductivity, free energy curves derived using calorimetry.

(c) A description of the purpose of the program, references to the science behind the algorithm, statement of the computer language used, the nature of the compilation where relevant (compiled versions are sensitive to the version of the compiler and to the operating system), explanation of the variables including the inputs and outputs, an example set of inputs and a corresponding example set of outputs, and the name and address of the originator of the code. The date and version of the software.

(d) The program could be written as follows:

```
      integer i,k
      real sum, a, fraction
      sum=0.0
      i=0

      do k=1,30
      read(*,*) a
        if(a .gt. 20.0 .and. a .lt. 40.0)then
          sum=sum+a
          i=i+1
        endif
        fraction=real(i)/30
      end do
      write (*,1) sum, fraction
1      format(2f10.2)
      end
```

(e) Major contribution comes from lattice vibrations; electrons make a minor contribution because the Pauli exclusion principle prevents all but a few from participating in the energy absorption process. Further contributions may come from magnetic changes or from ordering effects in general. As an example, the net specific heat capacity at constant pressure has the components:

$$C_P\{T\} = C_V^L\left\{\frac{T_D}{T}\right\}C_1 + C_e T + C_P^\mu\{T\}$$

where $C_V^L\{\frac{T_D}{T}\}$ is the Debye specific heat function and T_D is the Debye temperature. The function C_1 corrects $C_V^L\{\frac{T_D}{T}\}$ to a specific heat at constant pressure. C_e is the electronic specific heat coefficient and C_P^μ the component of the specific heat capacity due to magnetic effects.

(f) Diffusion is at first sight difficult to appreciate for the solid state. A number of mechanisms have been proposed historically. This includes a variety of ring mechanisms where atoms simply swap positions, but controversy remained because the strain energies associated with such swaps made the theories uncertain. One possibility is that diffusion occurs by atoms jumping into vacancies. But the equilibrium concentration of vacancies is typically 10^{-6}, which is very small. The theory was therefore not generally accepted until an elegant experiment by Smigelskas and Kirkendall.

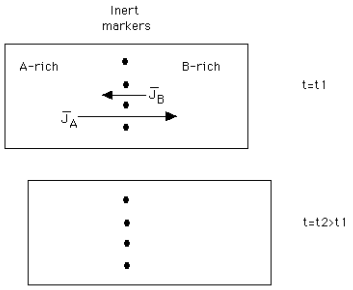

The experiment applies to solids as well as immiscible liquids. Consider a couple made from A and B. If the diffusion fluxes of the two elements are different ($|J_A| > |J_B|$) then there will be a net flow of matter past the inert markers, causing the couple to shift bodily relative to the markers. This can only happen if diffusion is by a vacancy mechanism.

(g) The physical reason why the growth rate decreases with time is apparent from the diagram below. Since in this case solute is being extracted from the matrix as the particle grows, the diffusion distance Δx increases in proportion to the particle size x. As a consequence, the concentration gradient decreases as the precipitate thickens, causing a reduction in the growth rate.

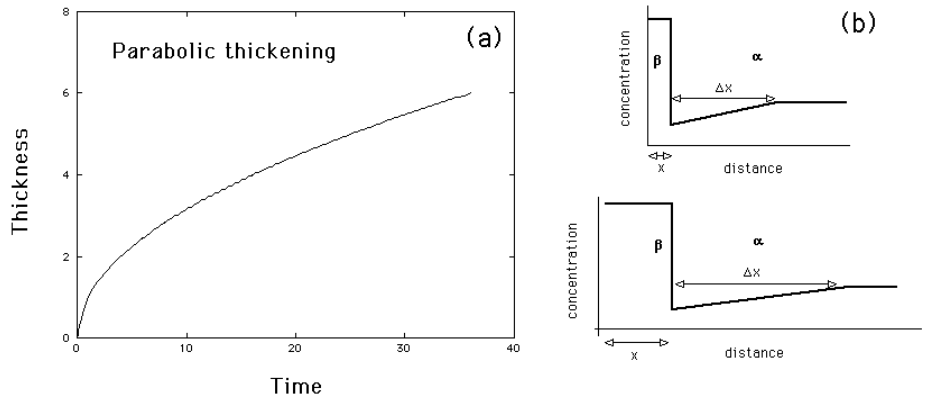

(h) The output y in a neural network is represented as a non–linear function of the inputs x_j. The function usually chosen being the hyperbolic tangent because of its flexibility. The exact shape of the hyperbolic tangent can be varied by altering the weights (Fig. 1a). Further degrees of non–linearity can be introduced by combining several of these hyperbolic tangents (Fig. 1b), so that the neural network method is able to capture almost arbitrarily non–linear relationship.

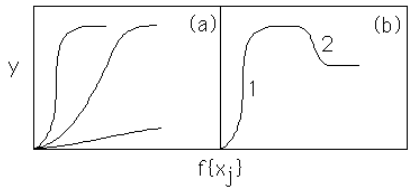

Fig. 1: (a) Three different hyperbolic tangent functions; the "strength" of each depends on the weights. (b) A combination of two hyperbolic tangents to produce a more complex model.

A potential difficulty with the use of powerful regression methods is the possibility of overfitting data (Fig. 2). For example, it is possible to produce a neural network model for a completely random set of data. To avoid this difficulty, the experimental data can be divided into two sets, a *training* dataset and a *test* dataset. The model is produced using only the training data. The test data are then used to check that the model behaves itself when presented with previously unseen data.

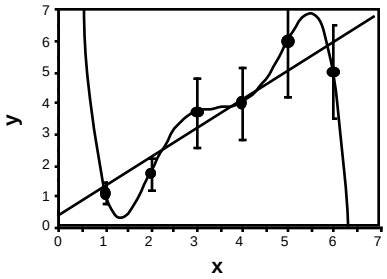

Fig. 2: A complicated model may overfit the data. In this case, a linear relationship is all that is justified by the noise in the data.

(i) Referring to the diagram below, the solid segments make up the first block (could be called 'A'), and the dashed segments the second block (could be called 'B'). The two main parameters are:

(i) the segment length a of A and B segments in terms of the number of monomers;

(ii) The interaction parameter χ (or the interaction energy E_{AB} between the two types of segments).

One expects a lamellar (sheetlike) structure.

Mean squared end–to–end distance scaling relationship: $R_L^2 \simeq N^x$, where N is the chain length, and x the scaling exponent.

For a phase separated diblock copolymer one expects the chains to be stretched out somewhat and therefore x to be larger than 1. (or a melt $x = 1$).

(j) Process modelling can improve process speed and quality and reduce costs, by providing: a means to explore new designs, reducing the need for practical trials (*e.g.* trial changes to shape of extrusion cross-sections); a means to try new operating regimes without loss of production (*e.g.* trial changes to starting block design in direct chill casting, or cooling schedules in extrusion of heat-treatable aluminium); support for re–design of equipment (*e.g.* modifying dies for extrusion); a physical basis for real-time control of processes (*e.g.* importance of avoiding surface melting in extrusion detrimental to finish); better process visualisation (*e.g.* temperature distribution within castings, metal flow in extrusion); prediction of microstructure and properties of final product, both average properties and variability (*e.g.* strength distribution across extrusions or welds in heat-treatable aluminium alloys); greater understanding of origins of failure - both during processing and later in service (*e.g.* hot tearing in castings, embrittlement of HAZ in carbon steel welds, distortion in extrusion, residual stress and distortion in welding).

SECTION B

2. Consider an alloy consisting of two components A and B. For the phase α, the free energy will in general be a function of the mole fractions $(1-x)$ and x of A and B respectively:

$$G^{\alpha} = (1-x)\mu_A + x\mu_B \tag{1}$$

where μ_A represents the mean free energy of a mole of A atoms in α. The term μ is called the *chemical potential* of A, and is illustrated in Fig. 3a. Thus the free energy of a phase is simply the weighted mean of the free energies of its component atoms.

Consider now the coexistence of two phases α and γ in our binary alloy. They will only be in equilibrium with each other if the A atoms in γ have the same free energy as the A atoms in α, and if the same is true for the B atoms:

$$\mu_A^{\alpha} = \mu_A^{\gamma} \qquad \text{and} \qquad \mu_B^{\alpha} = \mu_B^{\gamma}$$

If the atoms of a particular species have the same free energy in both the phases, then there is no tendency for them to migrate, and the system will be in stable equilibrium if this condition applies to all species of atoms.

The condition the chemical potential of each species of atom must be the same in all phases at equilibrium is general and justifies the common tangent construction illustrated in Fig. 3b.

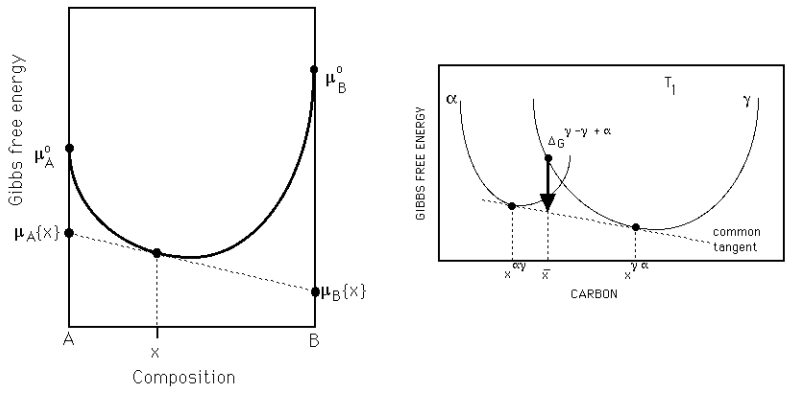

Fig. 3: Chemical potentials and the common tangent

Fick's first law is empirical in that it assumes that the diffusion flux is proportional to a concentration gradient. It would be more reasonable to assume that diffusion occurs in order to minimise the free energy so that the flux should be driven by a gradient of free energy:

$$J_A = -M_A \frac{\partial \mu_A}{\partial x} \qquad \text{so that} \qquad D_A = M_A \frac{\partial \mu_A}{\partial C_A}$$

where the (positive) proportionality constant M_A is known as the mobility of A. In this equation, the diffusion coefficient is related to the mobility by comparison with Fick's first law.

If $\partial\mu_A/\partial C_A > 0$ then the diffusion coefficient is positive and the chemical potential gradient is along the same direction as the concentration gradient. However, if $\partial\mu_A/\partial C_A < 0$ then the diffusion will occur against a concentration gradient. The diffusion coefficient will be zero when $\partial\mu_A/\partial C_A = 0$.

3. A Gaussian chain is given by the fact that distribution function for the end–to–end distance is a Gaussian. In other words the chain of length N can be regarded as a random walk of N steps. This means in terms of orientational correlations that the direction of each bond is completely independent of that of the previous bond.

   Two models are: Dissipative Particle Dynamics (DPD), and Mesoscale Ensemble Dynamics (MesoDyn).

   Key features; DPD: particle based, soft non–bonded interaction potential, pairwise interactions-momentum conservation, energy dissipation, random noise (Brownian). MesoDyn: concentration field based, free energy functional based, stochastic diffusion equation, mean field (Flory–Huggins) interactions.

   General expression for the time step:

$$\tau_R \ll \Delta t < \gamma^{-1}$$

   Here τ_R is the relaxation time of the atomistic processes, which bring about the mesoscale motion.

   There should be many such processes per timestep, so that the process will relax on the mesoscale time. Δt is the time step for the mesoscale simulation. γ^{-1} is the time related to the diffusion of the mesoscale segments (particles or beads). A typical time can be derived from the square of segment length divided by the diffusivity:

$$\gamma^{-1} \simeq l^2/D = 10^{-7}\,\mathrm{s} = 100\,\mathrm{ns}$$

   Since $\tau_R = 10^{-11}\,\mathrm{s} = 0.01\,\mathrm{ns}$, and the timestep should be much larger than that but smaller than 100 ns A lower bound would be about 1 ns, and an upper bound about 10 ns.

4. An estimation of the volume fraction requires *impingement* between particles to be taken into account. This is done using the extended volume concept of Kolmogorov, Johnson, Mehl and Avrami. Referring to Fig. 4, suppose that two particles exist at time t; a small interval δt later, new regions marked a, b, c & d are formed assuming that they are able to grow unrestricted in extended space whether or not the region into which they grow is already transformed. However, only those components of a, b, c & d which lie in previously untransformed matrix can contribute to a change in the real volume of the product phase (α) :

$$dV^{\alpha} = \left(1 - \frac{V^{\alpha}}{V}\right) dV_e^{\alpha} \tag{2}$$

where it is assumed that the microstructure develops at random. The subscript e refers to extended volume, V^{α} is the volume of α and V is the total volume. Multiplying the change in extended volume by the probability of finding untransformed regions has the effect of excluding regions such as b, which clearly cannot contribute to the real change in volume of the product.

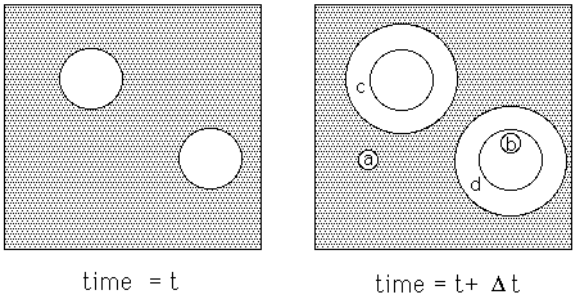

Fig. 4: The concept of extended volume.

The extended volume V_e^{α} is straightforward to calculate using nucleation and growth models and neglecting completely any impingement effects. Consider a simple case where the α grows isotropically at a constant rate G and where the nucleation rate per unit volume, I_V. The volume of a particle nucleated at time $t = \tau$ is given by

$$v_{\tau} = \frac{4}{3}\pi G^3 (t - \tau)^3$$

The change in extended volume over the interval τ and $\tau + d\tau$ is

$$dV_e^{\alpha} = \frac{4}{3}\pi G^3 (t - \tau)^3 \times I_V \times V \times d\tau$$

On substituting into equation 2 and writing $\xi = V^\alpha/V$, we get

$$\begin{aligned} dV^\alpha &= \left(1 - \frac{V^\alpha}{V}\right)\frac{4}{3}\pi G^3 (t-\tau)^3 I_V V \quad d\tau \\ \text{so that} \qquad -\ln\{1-\xi\} &= \frac{4}{3}\pi G^3 I_V \int_0^t (t-\tau)^3 \, d\tau \\ \text{and} \qquad \xi &= 1 - \exp\{-\pi G^3 I_V t^4/3\} \end{aligned} \tag{3}$$

5. The shear lag model is based on an analysis of the way in which axial stress is transmitted into the fibre via shear loading of the cylindrical surface of the fibre. Balancing shear and axial forces gives the basic equation of the model, which relates the gradient of axial stress (σ_i) in the fibre to the interfacial shear stress (τ_i) and fibre radius r:

$$\frac{d\sigma_i}{dx} = \frac{2\tau_i}{r}$$

The maximum stress that can be generated in the fibre is given when the interfacial shear stress along the whole of the half–length of the fibre has reached a plateau value of τ_{i*}, corresponding either to the shear yield stress of the matrix or to an interfacial shear strength. When the fibre length is such that this maximum stress is equal to the fracture stress of the fibre, σ_{f*}, then this represents the shortest fibre which could be fractured, with a half–length L_* such that

$$\frac{d\sigma_f}{L} = \frac{2\tau_{i*}}{r}$$

and the critical aspect ratio is given by

$$\frac{L_*}{r} = \frac{\sigma_{f*}}{2\tau_{i*}}$$

The expression assumes that all fibres debond rather than fracturing in the crack plane. This will occur provided that fibre aspect ratio is less than the critical value.

SECTION C

6. Bonding in molecular solids (examples: solid inert gases and also complex inorganic molecules although the bonding within the molecules is covalent).

Atoms have spherical electron distributions (full shells). Quantum mechanical screening effects cause fluctuations in the distribution. Atoms induce dipole moments in each other. This results in a weak attractive potential (known as van der Waals potential). The attractive potential is balanced by a weak repulsive interaction due to charge overlap.

Attractive $-1/r^6$ term can be justified from simple electrostatics. The dipoles induce an electric field $E \propto 1/r^3$. The energy of a dipole in an electric field $\propto -E^2$. The mutual energy of two dipoles $\propto -1/r^6$. The repulsive $1/r^{12}$ term has no physical justification. It is suggested by experimental data, *e.g.* viral coefficients.

The potential is valid for non–ionic solids which have spherical electron distributions, *i.e.* the potential is radially symmetric and pairwise. It has been used with some success for solid, liquid and gas phases of Lennard-Jonesium. Also binary compounds and for the simulation of defects.

Computationally it is not expensive because it is radial, pairwise and short range. Thus it has been used to simulate model sizes of around 1 billion atoms.

At equilibrium

$$\left(\frac{du}{dr}\right)_{r=r_0} = 0$$

where r_0 is the equilibrium nearest neighbour separation. Thus, for the f.c.c. structure,

$$-2\epsilon\left[12 \times 12.13 \times \frac{\sigma^{12}}{r_0^{13}} - 6 \times 14.45 \times \frac{\sigma^6}{r_0^7}\right] = 0$$

$$\textit{i.e.} \qquad \left(\frac{\sigma}{r_0}\right)^6 = \frac{14.45}{2 \times 12.13}$$

For the b.c.c. structure

$$-2\epsilon\left[12 \times 9.11 \times \frac{\sigma^{12}}{r_0^{13}} - 6 \times 12.25 \times \frac{\sigma^6}{r_0^7}\right] = 0$$

$$\textit{i.e.} \qquad \left(\frac{\sigma}{r_0}\right)^6 = \frac{12.25}{2 \times 9.11}$$

It follows that the equilibrium cohesive energy for the f.c.c. structure is

$$u(r_0) = 2\epsilon\left[12.13 \times \left(\frac{14.45}{2 \times 12.13}\right)^2 - 14.145 \times \frac{14.45}{2 \times 12.13}\right] = -\frac{14.45^2}{2 \times 12.13}\epsilon$$

Similarly, for the b.c.c. structure

$$u(r_0) = -\frac{12.25^2}{2 \times 9.11}\epsilon$$

Therefore,

$$\frac{u(\text{f.c.c.}) - u(\text{b.c.c.})}{u(\text{f.c.c.})} = 0.04$$

The two principal atomistic techniques covered in lectures were isobaric–isothermal (NpT) Monte Carlo (MC) and molecular dynamics (MD). Students may choose to outline either of these, and must then contrast the two.

The relevant thermodynamic state functions are the particle number N, the pressure p and the temperature T, which are all fixed, and the Gibbs free energy G, which is minimised during the transformation. It is essential that the cell volume V be allowed to vary, so that the increase in density in going from a b.c.c. to an f.c.c. structure (approximately 8.8%) can be accommodated, and that the temperature T is kept fixed to allow the potential energy liberated by the transformation to be released from the system. Students should comment on the use of periodic boundary conditions to mimic a bulk transformation, and superior answers would also include cell shape variation, using the Parinello–Rahman scheme, and the effects of finite size. Using larger periodic cells of fixed shape (usually cubic) will tend to inhibit the transformation.

A suitable algorithm for the NpT MC simulation would be a standard Metropolis acceptance scheme, supplemented by trial moves in the cell volume. Marks are allocated for identifying each of the following steps of the MC algorithm: (i) start with initial b.c.c. structure, (ii) generate trial configuration using either atomic translation or change in cell volume, (iii) accept trial configuration with probability $\min[1, \exp\{-\hat{a}\Delta H\}$, where ΔH is the enthalpy change (not expected to quote an explicit formula for ΔH). The efficiency of the algorithm may be improved by sampling changes in the cell volume only every $1/N$ steps (where N is the particle number), or by implementing non–local trial moves (for example, moving clusters of atoms).

A suitable algorithm for the NpT MD simulation would be to use an extended Lagrangian method, such as the Nos-Hoover method, in which the cell volume and two frictional coefficients relating the instantaneous temperature and pressure to their equilibrium values are additional dynamical variables. Identify each of the following steps of the MD algorithm:

(i) start with initial b.c.c. structure, (ii) calculate forces on each atom, (iii) integrate the equations of motion for the dynamical variables. The efficiency of the algorithm may be improved by using a Verlet neighbour list for the force calculation, and that the fluctuations in temperature and pressure may be reduced by adjusting the thermostat and barostat relaxation times to achieve critical damping.

The advantages of using MC over MD are that the equilibration times will generally tend to be much faster, especially if non–local trial moves are used. However, the MC simulations will not give a reliable guide to the dynamical processes that occur during equilibration. So, MC should be used if the object is to obtain a phase diagram for the system, whereas MD should be used if the object is to study the kinetics of the transformation. The simulations differ from the ideal calculation in that they are done at finite temperature and pressure. Therefore, although the calculation shows that f.c.c. is lower energy than b.c.c., it gives no insight as to whether the transformation will occur under a given set of experimental conditions.

7. The atomic arrangement in a crystal can be altered either by breaking all the bonds and rearranging the atoms into an alternative pattern (*reconstructive* transformation), or by homogeneously deforming the original pattern into a new crystal structure (*displacive* transformation), Fig. 5.

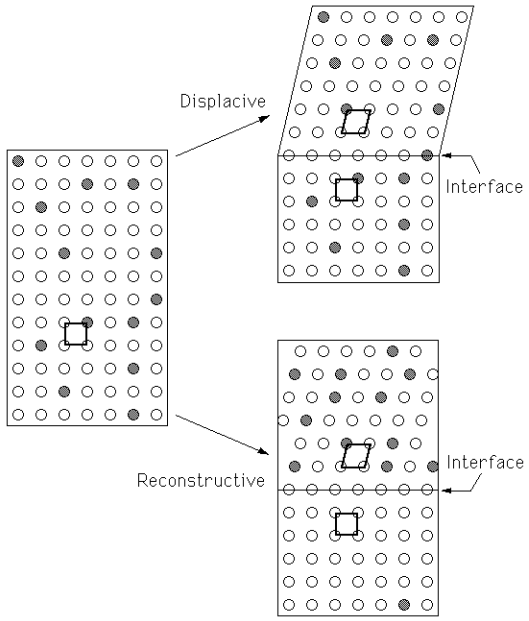

Fig. 5: The main mechanisms of transformation. The parent crystal contains two kinds of atoms. The figures on the right represent partially transformed samples with the parent and product unit cells outlined in bold. The transformations are unconstrained in this illustration.

In the displacive mechanism the change in crystal structure also alters the macroscopic shape of the sample when the latter is not constrained. The shape deformation during constrained transformation is accommodated by a combination of elastic and plastic strains in the surrounding matrix. The product phase grows in the form of thin plates to minimise the strains. The atoms are displaced into their new positions in a coordinated motion. Displacive transformations can therefore occur at temperatures where diffusion is inconceivable within the time scale of the experiment. Some solutes may be forced into the product phase, a phenomenon known as solute trapping. Both the trapping of atoms and the strains make displacive transformations less favourable from a thermodynamic point of view.

Fig. 6 shows how the shape of the product phase changes when the transformation is constrained, because a thin–plate then minimises the strain

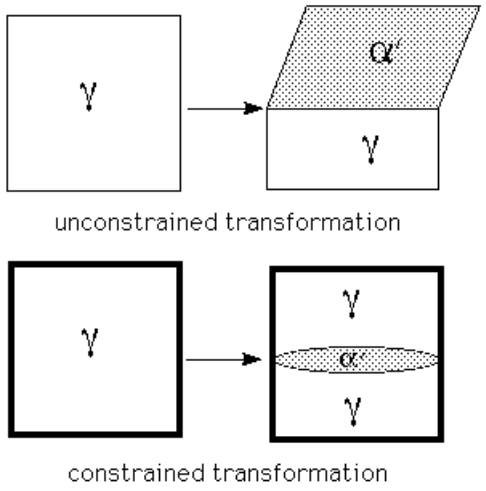

Fig. 6: The effect of strain energy on the morphology of the transformed phase during displacive transformation involving shear deformation.

energy.

It is the diffusion of atoms that leads to the new crystal structure during a reconstructive transformation. The flow of matter is sufficient to avoid any shear components of the shape deformation, leaving only the effects of volume change.

As the columnar austenite grains of the weld cool into the $\alpha + \gamma$ phase field, allotriomorphic ferrite layers nucleate and grow to decorate the prior austenite grain boundaries. This reconstructive transformation occurs with the diffusion of carbon and iron. As the temperature decreases, the diffusion of iron rapidly becomes difficult, giving rise to plates of Widmanstätten ferrite in which the change in crystal structure is achieved by a displacive mechanism, although carbon (which can still diffuse rapidly) is partitioned. Acicular ferrite, which nucleates intragranularly on oxide particles present in welds, grows by a displacive mechanism to form a desirable, chaotic microstructure which is good for toughness. Finally, martensite forms without any diffusion.

(i) All the displacive transformations, which do not require diffusion, are promoted by increasing the cooling rate.

(ii) $Q = IV\eta/s$ where I, V, η and s are the current, voltage, arc transfer efficiency and speed respectively. The cooling rate must naturally increase as Q decreases since less heat has to be dissipated into the environment. The cooling rate can be assumed to depend on the difference between the actual temperature T and the substrate temperature T_0, so the cooling

rate increases as T_0 decreases.

(iii) The theory describing diffusion controlled growth contains a dimensionless supersaturation

$$\Omega = \frac{C^{\gamma\alpha} - \overline{C}}{C^{\gamma\alpha} - C^{\alpha\gamma}}$$

where the two terms in the denominator refer to the equilibrium solubilities of carbon in austenite and in ferrite respectively. $\overline{C}$ is the average concentration. As $\overline{C} \rightarrow C^{\alpha\gamma}$, *i.e.* the average concentration approaches the solubility of carbon in ferrite, less solute is partitioned, making $\Omega \rightarrow 1$, so that diffusion–controlled growth becomes very rapid.